Oxidation of Metals (2022) 97:559–574
https://doi.org/10.1007/s11085-022-10108-4

ORIGINAL PAPER

Silicon Contamination During Alloy Oxidation in Water Vapour at 650 °C

Thuan Dinh Nguyen[1] · Jianqiang Zhang[1] · David J. Young[1]

Received: 13 February 2022 / Revised: 13 February 2022 / Accepted: 13 March 2022 /
Published online: 31 March 2022
© The Author(s) 2022

Abstract

A model Si-free alloy, Fe-30Cr (wt.%), was exposed to Ar-10H_2O mixture (in vol.%) at 650 °C, forming a protective Cr_2O_3 scale, which contained silica. Liquid water used to form water vapour in a bubbler was either deionised or distilled. In both cases, low-level water impurities of Si, F, Cl, S, and Ca matched those detected in the Cr_2O_3 scales by TEM/EDX and ToF–SIMS. Consideration of water droplet and residual solute particle sizes, together with Stokes' Law shows that entrainment of Si in the gas stream is likely. Calculation of mass transfer rates from the gas to the growing chromia scale show that the amount of silica in the scale is accounted for. Many laboratory experiments could be affected in this way.

Keywords Chromia formers · Water vapour · High-temperature corrosion · Si contamination

Introduction

Combustion of fossil fuels releases mainly CO_2 and water vapour. For this reason, the extensively studied high-temperature corrosion of commercial and model alloys in H_2O-containing gases is of practical relevance as well as fundamental interest. Corrosion resistance of these alloys usually relies on the formation of slow-growing scales of Cr_2O_3, Al_2O_3, or SiO_2. Alloys with sufficient Cr and Si concentrations oxidise in various gases to form a duplex scale of an outer Cr_2O_3 layer and a thin, inner SiO_2 layer [1–7]. This additional SiO_2 layer is beneficial in slowing growth of the overlying Cr_2O_3 layer and consequently Cr depletion in the alloy.

The SiO_2 layer is usually observed between the Cr_2O_3 layer and alloy, because SiO_2 is more stable. Alloy Si concentrations are rather small (less than 2 wt.%), but

✉ Jianqiang Zhang
j.q.zhang@unsw.edu.au

[1] School of Materials Science and Engineering, University of New South Wales, Sydney, NSW 2052, Australia

its diffusion in alloys is quite fast [1–6]. It has been reported that additional SiO_2 precipitates were detected within Cr_2O_3 scales on Fe-20Cr-0.5Si (all alloy compositions in wt. %) formed in Ar-20H_2O-20CO_2 [3, 4]. In a previous study [4], chromia scales formed in 380 h on a model Fe-20Cr alloy at 650 °C had different structures in wet and dry gases: relatively coarse, columnar grains in Ar-20CO_2 (Fig. 1a), but an inner layer of fine, equiaxed grains surmounted by Cr_2O_3 blades on the scale surface in Ar-20CO_2-20H_2O (Fig. 1b). Surprisingly, recent EDX analysis shows that silicon was detected in the chromia scale formed in wet CO_2 (Fig. 1d, e), but not for that in dry CO_2 (Fig. 1c).

Silicon-rich oxides have also been found on the surface of and inside an Al_2O_3 scale formed on FeCrAl-1.3Si alloy reacted in wet air at 800 °C [7]. In the case of chromia scales, the additional silica layer strengthens their protective effect and improves the alloy corrosion resistance significantly. The formation of additional SiO_2 precipitates in the Cr_2O_3 or Al_2O_3 layer was suggested to be due to the transport of Si from the underlying alloy to the surface [3, 7].

In the present work, a model Si-free alloy of Fe-30Cr was reacted with Ar-10H_2O (volume %) at 650 °C. The aim was to study contamination by silicon and other elements during high-temperature oxidation in water vapour. The results would also help to understand the potential effects of these contaminations on corrosion behaviour in other wet gases.

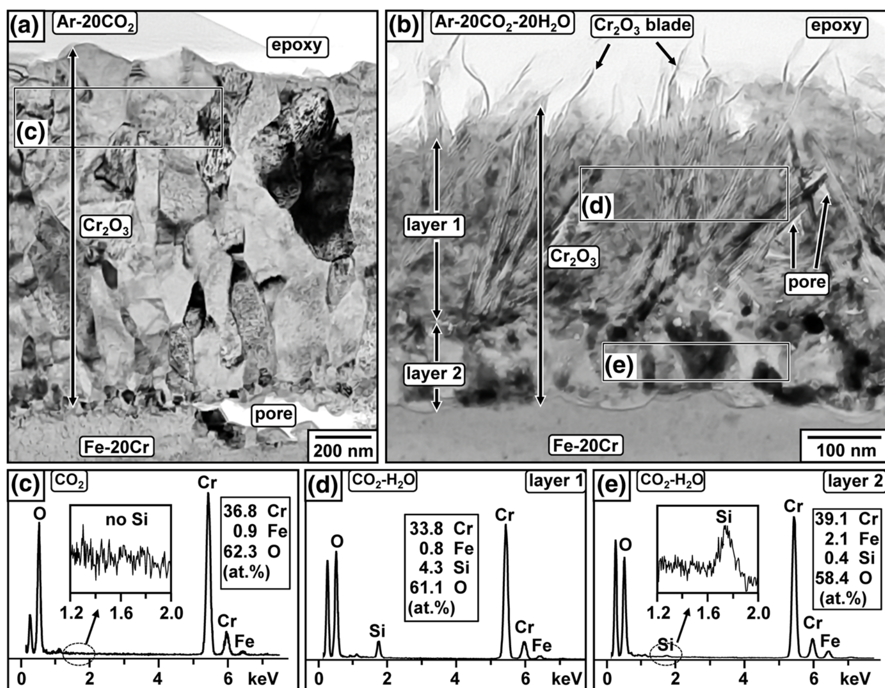

Fig. 1 BF-TEM cross-sections [4] and EDX spectra of selected areas of thin Cr_2O_3 scales formed on Fe-20Cr reacted in (a, c) Ar-20CO_2 and (b, d, e) Ar-20CO_2-20H_2O for 380 h using a distilled water source

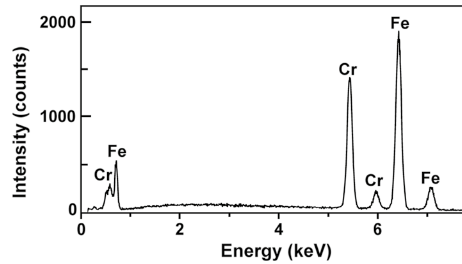

Fig. 2 SEM/EDX spectrum of as-received Fe-30Cr

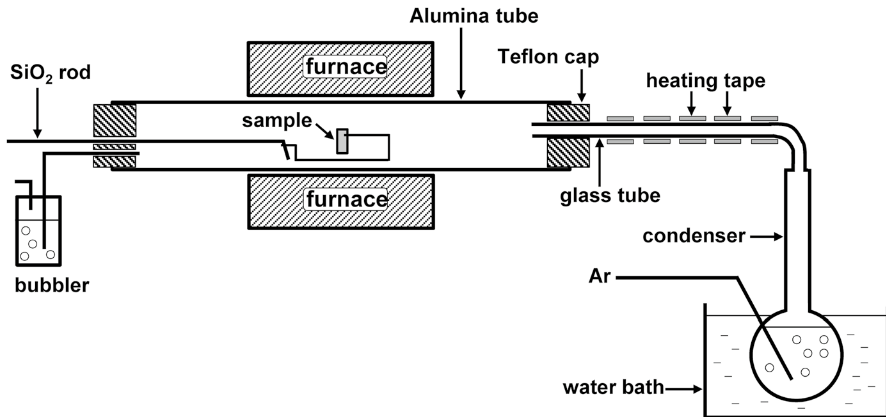

Fig. 3 Schematic illustration for experiments in Ar-10H_2O

Materials and Experiments

A model Fe-30Cr alloy (wt.%) was prepared by arc melting pure metals Fe (99.98% metals only basis) and Cr (99.995% metals only basis) under a protective Ar-5%H_2 (volume %) gas atmosphere, using a non-consumable electrode. The resulting button was annealed at 1000 °C for 70 h in a flowing Ar-5%H_2 gas for homogenization. Rectangular alloy coupons $(1\pm0.1)\times(8\pm0.2)\times(8\pm0.2)$ mm in size were surface ground to a 1200-grit finish and ultrasonically cleaned in ethanol prior to reaction. The alloy composition was checked by SEM/EDX (Fig. 2) and found to be Fe-(29.8 ± 0.1)Cr (wt.%). No Si peak was observed in the spectrum, showing the alloy to contain less than the detection limit of about 0.1 wt.%. Further ICP analysis confirmed a very low concentration of Si impurity, about 0.002 wt.%.

All specimens were reacted at 650 °C in Ar-10H_2O mixture (volume %) with a linear flow rate of 1 cm/s and a total pressure of 1 atm for up to 240 h. A horizontal alumina tube furnace was used, and the experimental setup is shown in Fig. 3. The Ar gas was flowed at controlled rates through a flask containing water at a controlled temperature, yielding the desired partial pressures of H_2O. The flask was filled with deionised water (Sartorius, arium-pro). Heating tapes set at 88 °C

were used to prevent condensation inside glass tubes connecting the condenser to the reactor tube's end cap.

No silicone grease was used at glassware joints to avoid potential Si contamination from this source. Alloy samples were suspended in an alumina crucible using Kanthal alloy wire.

Corroded samples were characterized by X-ray photoelectron spectroscopy (XPS, ESCALAB250Xi-Thermo Scientific), scanning electron microscopy (SEM, Hitachi S3400) with an energy dispersive X-ray spectrometer (EDX, Bruker), and transmission electron microscopy (TEM, JEOL JEM-F200). The TEM samples were prepared using a focused ion beam system (FIB, FEI Nova Nanolab 200) with a maximum accelerating voltage of 30 kV. Scale contaminants on the oxidised samples were analysed mainly by time-of-flight ion mass spectrometry (ToF–SIMS, TOF. SIMS5-IONTOF). A sputter area of $300 \times 300\ \mu m^2$ was formed by a Cs + ion beam (1 keV, 70.9 nA). A Bi^+ ion beam (30 keV, 2.6 pA) was used for negative ions profiles and Bi^{3+} for positive ions profiles. The analysis area was $100 \times 100\ \mu m^2$. For ToF–SIMS analysis, samples were oxidised in the alumina tube with aluminium end caps to avoid any possible contamination from the Teflon cap.

Results

The scale formed on Fe-30Cr in Ar-10H_2O consisted of fine, equiaxed grains at its surface (Fig. 4). Analysis by STEM/EDX mapping (Fig. 5a, b) and spectra (Fig. 5c–e) shows the thin, dense scale (about 240 nm thick) to be Cr_2O_3. A pore was also found beneath this Cr_2O_3 scale, located at an alloy grain boundary (Fig. 5a).

A small amount of Si (0.2 at.%) was detected in the oxide scale, e.g. area (c) in Fig. 5a, but not everywhere, e.g. at points 1 and 2 of coarse oxide grains

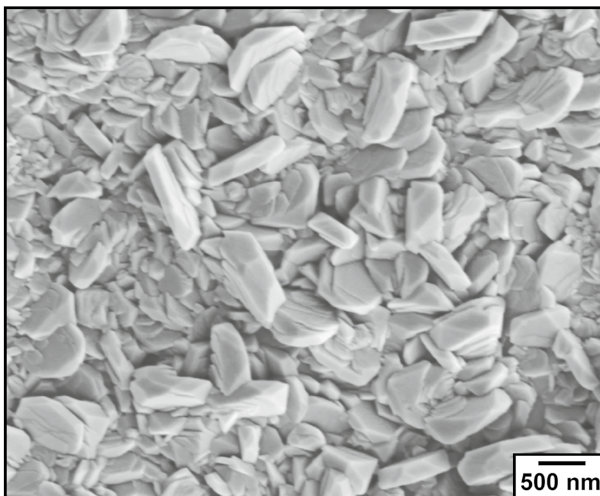

Fig. 4 SE-SEM top view of Fe-30Cr reacted in Ar-10H_2O (deionised water source) for 240 h

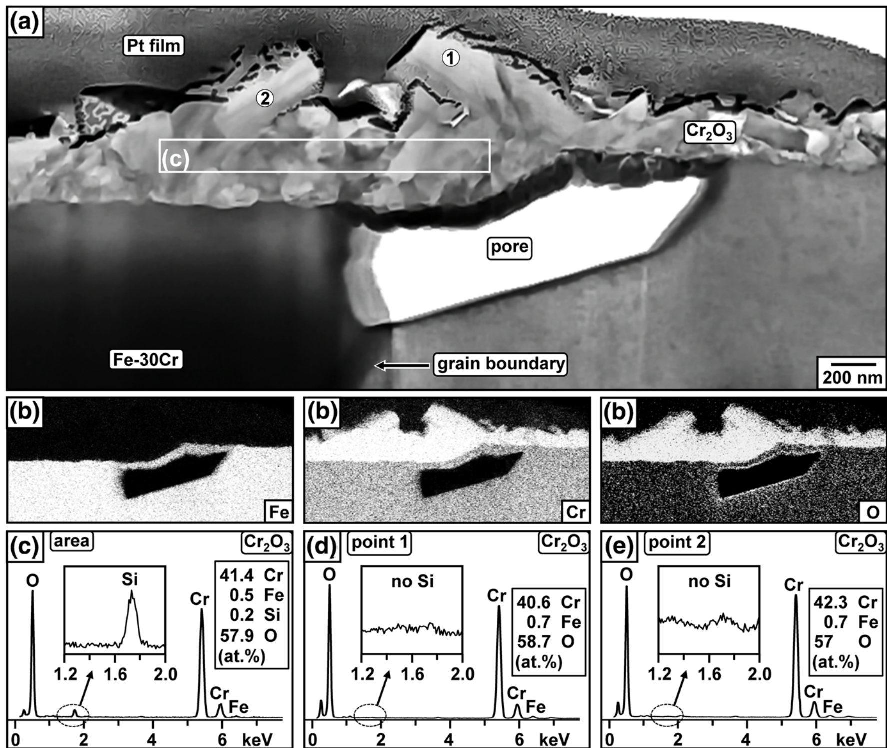

Fig. 5 Fe-30Cr reacted in Ar-10H_2O (deionised water source) for 240 h: **a** BF-STEM cross-section, **b** EDX mapping, and EDX spectra of the scale: **c** area, **d** point 1 and **e** point 2

(Fig. 5a,d,e). The chemical state of silicon in the Cr_2O_3 scale was analysed by XPS (Fig. 6). The $Cr_{2p3/2}$ peak centred at 577.16 eV matches with the $Cr_{2p3/2}$ binding energy in Cr_2O_3 [8]. The Si_{2p} peak centred at 102.14 eV matches with the Si_{2p} binding energy in SiO_2 [8]. The Si spectrum was weaker than that of Cr because of its lower concentration.

The ToF–SIMS depth profiles obtained from the scale on Fe-30Cr oxidised in Ar-10H_2O (deionised water) for 20 h (Fig. 7) show that ions of Si, F, Cl, S, and Ca were detected in the Cr_2O_3 scale. Part of these impurities, Si and Ca were concentrated

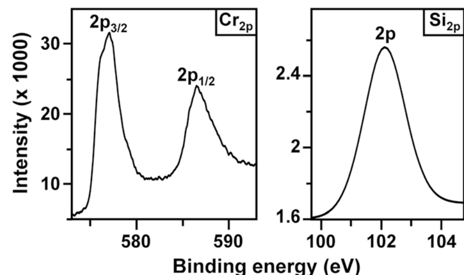

Fig. 6 Fe-30Cr reacted in Ar-10H_2O (deionised water source) for 240 h: XPS spectra of Cr_{2p} and Si_{2p} taken from the surface

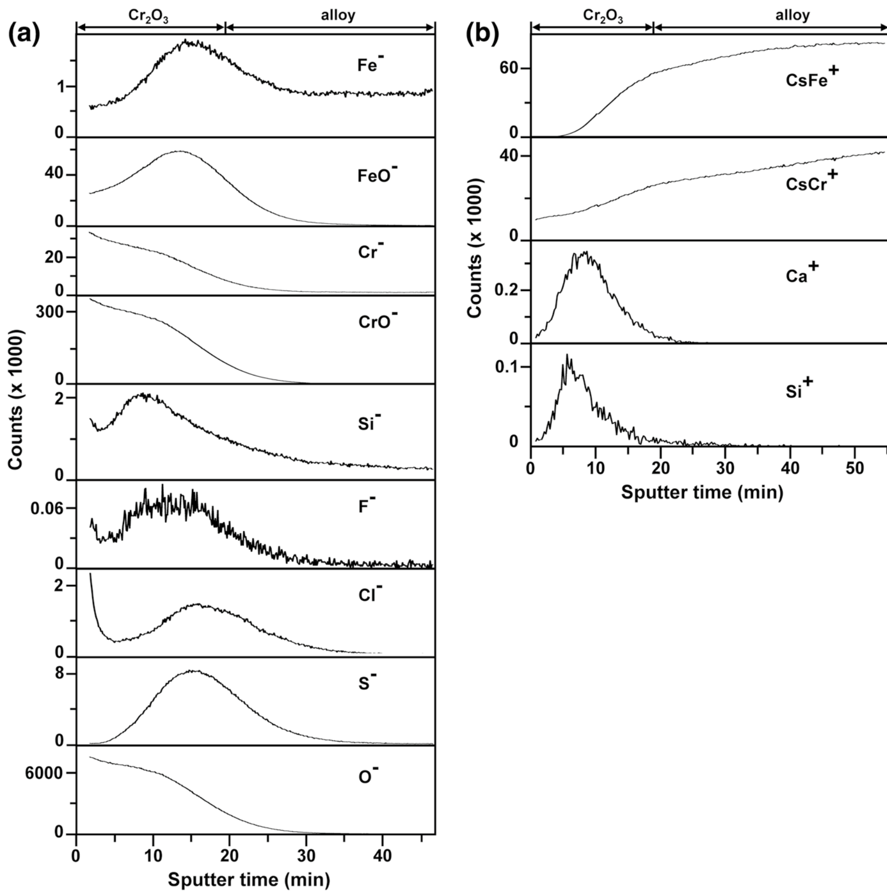

Fig. 7 ToF–SIMS analysis of Fe-30Cr oxidized in Ar-10H_2O (deionised water source) for 20 h using a primary ion beam of (**a**) Bi^+ for negative polarity profiles and **b** Bi^{3+} for positive polarity profiles. Cs in (**b**) from the sputter ion source

mainly in outer parts of the scale, whereas F, Cl and S appeared throughout the oxide. In addition, FeO^- was found to be present at the middle of the chromia, possibly derived from Fe–Cr-spinel.

An experiment with Ar-10H_2O using distilled liquid water was carried out to compare scales grown with deionised and distilled water. The ToF–SIMS depth profiles of the Cr_2O_3 scale formed in Ar-10H_2O (distilled water) in Fig. 8 show impurities of Si, F, Cl, S, and Ca. The detection of Si^-, Si^+, F^-, Cl^-, S^-, and Ca^+ ions in both experiments is a surprise, and is now considered.

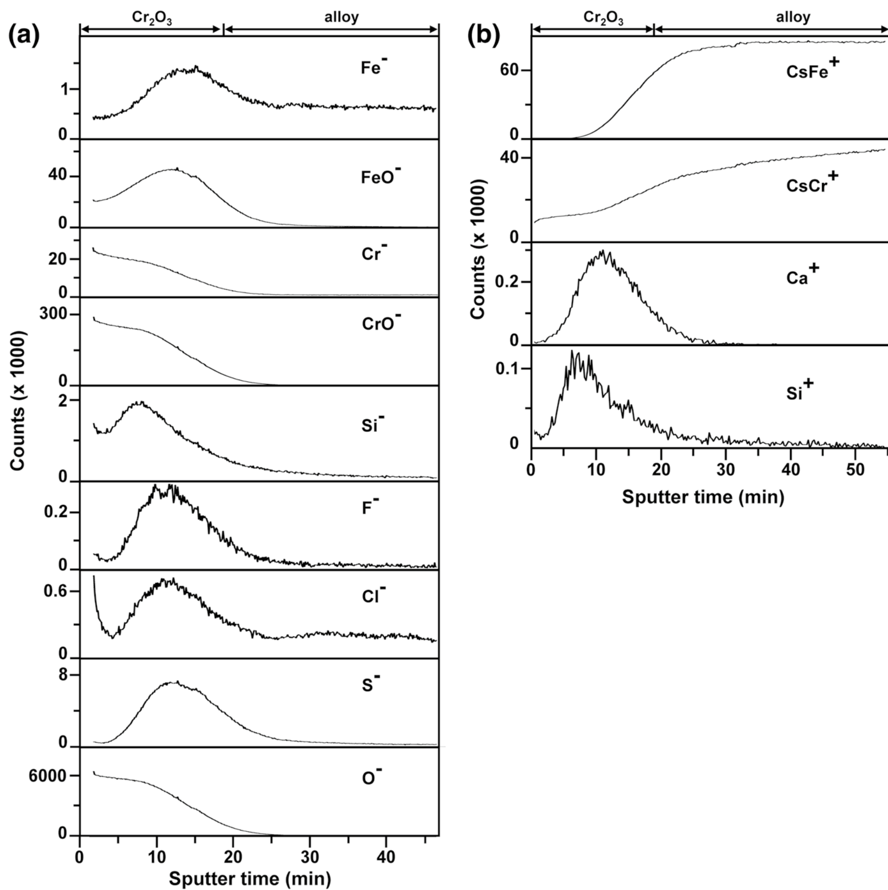

Fig. 8 ToF–SIMS analysis of Fe-30Cr oxidized in Ar-10H_2O (distilled water source) for 20 h using a primary ion beam of (**a**) Bi^+ for negative polarity profiles and **b** Bi^{3+} for positive polarity profiles. Cs in (**b**) from the sputter ion source

Discussion

Origin of Si Contamination in Water Vapour Oxidation

The presence of silicon in the chromia scale after oxidation in Ar-10H_2O is a big surprise. The experiment was carried out in an alumina tube instead of a silica tube, eliminating possible interactions between the reaction tube and water vapour at high temperatures. The silica rod used to insert and retract samples (Fig. 3) was behind the sample at the gas downstream side, minimising any possible contamination from reactions between silica and the reaction gas.

It has been reported that solid SiO_2 could react with steam (0.8 atm) at 800 °C [9] and a gas mixture of water vapour and oxygen (1 atm) at 1200 °C [10], forming volatile hydroxides:

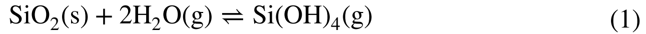

$$SiO_2(s) + 2H_2O(g) \rightleftharpoons Si(OH)_4(g) \tag{1}$$

with a standard Gibbs free energy change of [11, 12]

$$\Delta G^o = 52300 + 76.79T \quad (J/mol) \tag{2}$$

Another possible volatile Si-bearing gas could be formed by the reaction:

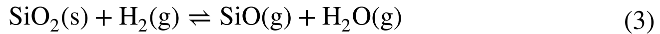

$$SiO_2(s) + H_2(g) \rightleftharpoons SiO(g) + H_2O(g) \tag{3}$$

with a standard Gibbs free energy change of [11]

$$\Delta G^o = 568700 - 228.5T \quad (J/mol) \tag{4}$$

The maximum partial pressures of $Si(OH)_4$ (g) and SiO (g) were calculated from Eqs. (2, 4) using $p_{H_2O} = 0.1$ atm and $p_{H_2} = 1\times10^{-8}$ atm (partial pressures of water vapour and H_2 in reaction gas) and unit SiO_2 activity are $p_{Si(OH)_4} = 1.1\times10^{-9}$ atm and $p_{SiO} = 6.1 \times 10^{-29}$ atm. It is clear that Si contamination from the SiO_2 rod was very low and the Si contamination came from the alloy and/or reaction gas (water vapour).

Effect of Si Impurity in Alloy

The total amount of Si in the chromia scale is

$$n_{Si}^{scale} = \frac{N_{Si}}{N_{Cr}} n_{Cr}^{scale} \tag{5}$$

where N_{Si} and N_{Cr} are average concentrations (atom %) of Si and Cr in the chromia scale measured by TEM/EDX analysis, and n_i^{scale} the amount of indicated component per unit surface area in the scale (mol/cm^2). Approximating the scale formed on Fe-30Cr as pure Cr_2O_3

$$n_{Cr}^{scale} = 2\frac{\delta_{Cr_2O_3}\rho_{Cr_2O_3}}{M_{Cr_2O_3}} \tag{6}$$

where $\rho_{Cr_2O_3}$ and $M_{Cr_2O_3}$ are density and molar mass of Cr_2O_3, and $\delta_{Cr_2O_3}$ the average chromia scale thickness. The average $\delta_{Cr_2O_3}$ value is 240 nm (Fig. 5), yielding $n_{Si}^{scale} = 8.1 \times 10^{-9}$ mol/cm^2.

The Si concentration in the alloy is $C_o = 0.002$ wt.% obtained from the ICP measurement. The total amount M_t of Si transported from a thin sheet, with a thickness of $2\ell = 1$ mm, to a surface at which the alloy Si concentration is set at zero is calculated from [13]:

$$\frac{M_t}{M_\infty} = \frac{1}{2}\left[1 - \sum_{n=0}^{\infty} \frac{8}{(2n+1)^2\pi^2} \exp\left(\frac{-D_{Si}(2n+1)^2\pi^2 t}{4\ell^2}\right)\right] \tag{7}$$

Here $M_{\infty}=2.1\times10^{-7}$ mol/cm^2 is the initial Si amount in Fe-30Cr,$D_{Si}=3.1\times10^{-13}$ cm^2/s [14], t time (s). Using the graphical solution provided by [13], it is found for $t=240$ h that $M_t/M_{\infty}=0.005$. The calculated M_t value of Si for 240 h is 1.1×10^{-9} mol/cm^2, significantly smaller than the Si amount in the Cr_2O_3 scale of $n_{Si}^{scale}=8.1\times10^{-9}$ mol/cm^2. It is therefore concluded that Si impurity in the alloy was not the main Si source for the formation of silicon oxide within the Cr_2O_3 scale grown in Ar-10H_2O.

The remaining possible Si source is the reaction gas. The shape of the Si profiles within the chromia scales (Figs. 7, 8), with their high concentrations near the scale surface, supports the view that silicon enters the oxide from its interface with the gas. Moreover, Fe-20Cr alloy, when exposed to dry CO_2 (Fig. 1), oxidised to form a Cr_2O_3 scale containing no detectable level of silicon, but developed a scale containing Si when H_2O(g) was added to the environment. This pattern of behaviour is readily understood if water was the source of silicon. The latter explanation is now examined.

Transport of Si Impurity by Water Vapour-Containing Gases

Tap water usually contains impurities as shown in Table 1. Tap water in our laboratory was analysed by ICP-OES to contain about 1.29 mg/L silicon, in agreement with a result from the water supplier in Sydney of 0.7 ~ 1.68 mg/L [15]. Sources of Si in tap water can be natural weathering of mineral matter or human activity (water fluoridation). Fluoride is commonly added to water sources for dental health reasons. The fluoride level in Sydney water is about 1.02 mg/L [16]. The most common fluoride compound used in New South Wales (Australia) is sodium silicofluoride (Na_2SiF_6) for large water supplies, and sodium fluoride (NaF)/hydrofluosilicic acid (H_2SiF_6) for medium to small water supplies [16]. The detection of low levels of F in the Cr_2O_3 scales (Figs. 7, 8) which contained silicon is consistent with the view that fluoridation with Na_2SiF_6 is the ultimate source of silicon contamination.

Silicon is one of the most abundant elements on earth, and can be found in large amounts in rivers and the sea. Weathering of Si-containing minerals results in dissolved silicon in the form of silicic acid $Si(OH)_4$ [17]. The world average concentration of dissolved Si in rivers is about 4.2 mg/L [17]. As is seen, the concentration

Table 1 Main impurities in Sydney drinking water [15]

	mg/L
Calcium	11.5 ~ 16.5
Chloride	30 ~ 31.5
Fluoride	1
Magnesium	2.6 ~ 7.3
Potassium	2.6 ~ 3.2
Sodium	14.8 ~ 20.4
Sulfate	8.4 ~ 11
Si	0.7 ~ 1.68

of dissolved Si in tap water caused by water fluoridation and mineral weathering is small, and is generally disregarded in corrosion research reports.

For water vapour experiments, tap water was deionised using a Sartorius Arium-pro ultra-pure lab water system. An ICP-OES analysis (Table 2) indicated silicon concentrations in the deionised water to be 0.16 mg/L. The other main impurities of Ca, Cu, K, Mg, and Na were also still present. For comparison, the distilled water supply was also analysed (Table 2). It is clear that the deioniser and distiller had greatly improved water quality (Table 1), but had failed to remove dissolved Si and other impurities completely. These low residual impurity levels would be common in conventional laboratory experiments, but are ignored.

The question remains as to how these species were transferred from the liquid water through which gas was bubbled (Fig. 3), via the gas phase, resulting in their detection in the reaction product Cr_2O_3 scales (Figs. 5, 6, 7, 8).

The transport of impurity species from liquid water into the flowing gas at the low temperature of the bubbler flask could occur, at least in principle, via chemical and physical processes. Any contribution of salt vaporisation can be dismissed. Water vapour was formed by bubbling Ar gas in the heated flask containing liquid water, resulting in the Ar-10H_2O mixture with an equilibrium saturation temperature of 45.8 °C [18]. Equilibrium vapour pressures of the dilute solute salts, which have high melting points, would be negligible at this temperature.

However, the dry Ar gas was injected at the water flask bottom, forming bubbles (Fig. 3). When these bubbles burst at the gas–water interface, very small water droplets containing dissolved impurity species are ejected, forming an aerosol [19–21]. Subsequent evaporation of water from these droplets would leave solid salt particles. The size of bubbles depends on many factors: inner diameter of gas tube, gas flow rate, water density/viscosity, wetting property of gas tube, and water height above the tube outlet. It has been reported [22] that bursting a bubble with a diameter of 3.95 mm formed a majority of droplets with a diameter of about 20 ~ 40 μm. On this basis, approximating the bubble diameter as equal to the inner diameter of the gas tube, 4.6 mm, the resulting droplet diameters would be up to 40 μm.

An approximate calculation shows that these residual particles are likely to be very small. A water droplet of 3.3×10^{-5} mm^3 with a total dissolved solids level of about

Table 2 Concentrations (mg/L) of main impurities in distilled and deionized water by ICP analysis

	Deionized water (mg/L)	Distilled water (mg/L)	Detection limit (mg/L)
Ca	0.132	0.021	0.002
Cu	0.006	0.0002	0.0002
K	0.096	0.067	0.002
Mg	0.055	0.002	0.002
Na	0.504	0.684	0.002
S	0.05	-	0.05
Si	0.167	0.161	0.002
F	-	-	0.05
Cl	0.319	-	0.2

1 mg/L (Table 2) contains about 3.3×10^{-14} g of solute. Approximating the solid density to be that of NaCl, 2.17 g cm^{-3}, it is calculated that if the solute formed a single spherical particle, its maximum diameter would be about 0.3 μm. The possibility that water droplets or salt particles could be carried upward by the flowing gas is now considered.

The terminal velocity (v_T) of a falling spherical droplet/particle in a viscous fluid is described by Stokes' law.

$$v_T = \frac{2(\rho_{droplet} - \rho_{gas})g\, r^2}{9\eta} \tag{8}$$

Here $\rho_{droplet}=1000$ kg m^{-3} and $\rho_{gas}=1.69$ kg m^{-3} are the mass densities of water and Ar gas, $g=9.81$ m s^{-2}, r radius of water droplet or particle, and $\eta=2.4\times10^{-5}$ kg m^{-1} s^{-1} is the dynamic viscosity of Ar gas at 50 °C [23].

The average Ar gas velocity in the gas space above the water surface in the flask filled with one litre of water at 45.8 °C is $v_{gas}=0.13$ cm s$^{-1}=13\times10^{-4}$ m s^{-1}. When $v_T = v_{gas}$, the critical value of $r^{droplet}$ calculated from Eq. (8) such that any smaller droplets could be carried upward by the gas is 3.8 μm (or 7.6 μm diameter). In the case of a spherical NaCl salt particle ($\rho_{salt}=2170$ kg m^{-3}), the critical r^{salt} value is 2.6 μm (or 5.2 μm diameter), much greater than the maximum diameter of a salt particle of 0.3 μm calculated above. It is concluded that the flowing Ar-10H_2O gas mixture could carry water droplets smaller than 7.6 μm from the bubbler into the heated reactor tube, along with solid solute residues from larger droplets after evaporation.

The ToF–SIMS results show that intensities of depth profiles of impurity ions are the same for the samples oxidised in either distilled or deionised water (Figs. 7, 8), except for F^- and Cl^-. The F^- concentrations in the two water supplies were below the detection limit of ICP analysis (Table 2), but the ToF–SIMs results show higher intensities for the F^- profile in the experiment with distilled water (Figs. 7, 8). The Cl^- concentration in deionised water was higher than that in distilled water (Table 2), resulting in higher intensities for the Cl^- profile in the scale formed from deionised water (Figs. 7, 8). This reinforces the conclusion that water vapour produced from liquid water is not absolutely pure and still contains significant amounts of the original impurities.

Mass Transfer of Si

The liquid water volume consumed during the 240 h reaction was about $V_{H_2O} = 0.373$ L, and the silicon concentration in the deionised water was 0.16 mg/L. If all the solute Si in the vapourised water was transported by the gas stream into the reactor, a total amount $n_{Si}^{gas} = 2.1 \times 10^{-6}$ mol was supplied during the 240 h reaction.

The overall reactions of Na_2SiF_6 and H_2SiF_6 in liquid water are [24]:

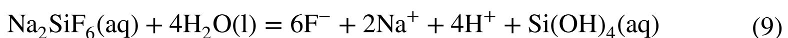

$$Na_2SiF_6(aq) + 4H_2O(l) = 6F^- + 2Na^+ + 4H^+ + Si(OH)_4(aq) \tag{9}$$

$$H_2SiF_6(aq) + 4H_2O(l) = 6F^- + 6H^+ + Si(OH)_4(aq) \tag{10}$$

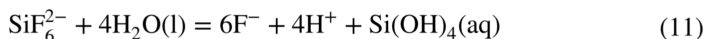

$$SiF_6^{2-} + 4H_2O(l) = 6F^- + 4H^+ + Si(OH)_4(aq) \tag{11}$$

The hydrolysis reaction (11) of Na_2SiF_6 or H_2SiF_6 has been shown to be rapid and complete, resulting in essentially no SiF_6^{2-} remaining in tap water at equilibrium [24]. It is concluded that the chemical state of most of the Si dissolved in water is $Si(OH)_4$.

Conversion of liquid water to water vapour results in a partial pressure of $Si(OH)_4$ gas $\left(p_{Si(OH)_4}\right)$ given by

$$p_{Si(OH)_4} = p_{H_2O}\frac{C_{Si}^{water}M_{H_2O}}{M_{Si}} \tag{12}$$

At the temperature employed, $p_{H_2O} = 0.1$ atm, $C_{Si}^{water} = 0.16$ mg Si/1L $H_2O = 16 \times 10^{-8}$ g Si/g H_2O in deionised liquid water, M_{H_2O} and M_{Si} are molar masses of H_2O and Si. The calculated value of $p_{Si(OH)_4}$ is 1×10^{-8} atm. This is an order of magnitude greater than the value estimated from a presumed equilibrium of Eq. (1).

However, the rate of the unimolecular gas phase reaction (1) to form SiO_2(s) is unknown, but probably slow. It will therefore be assumed that the actual value of $p_{Si(OH)_4}$ lies between a maximum value 1×10^{-8} atm, deriving from the input Ar-H_2O-$Si(OH)_4$ gas stream, and a minimum of 1.1×10^{-9} atm resulting if reaction (1) reaches equilibrium.

For laminar flow of gas over and parallel to a flat sample, a boundary layer of gas attaches to the sample surface. Mass transfer of Si from the bulk gas onto the sample surface is controlled by diffusion across the boundary layer, and may be calculated using gas transport theory in the viscous flow regime [25].

The deposition rate was calculated as a flux, J, from

$$J = \frac{k_m}{RT}p_{Si(OH)_4} \tag{13}$$

where k_m(cm/s) is the mass transfer coefficient and $p_{Si(OH)_4}$(atm) partial pressure of $Si(OH)_4$, and $T = 923$ K the gas temperature. The value of k_m is given by

$$k_m = 0.664\left(\frac{D_{AB}^4}{v_g}\right)^{1/6}\left(\frac{v}{L}\right)^{1/2} \tag{14}$$

where D_{AB} (cm^2s^{-1}) is the binary gas A-B diffusion coefficient, v_g the kinematic viscosity, $v = 1$ cm/s the linear gas velocity at 650 °C, and $L = 0.8$ cm the length of sample surface.

The reaction gas mixture was Ar-10H_2O-$Si(OH)_4$. A simplified model of a binary gas mixture of Ar-$Si(OH)_4$ was used. The necessary collision diameter and interaction energy data for $Si(OH)_4$ are not available, so values [26] for SiF_4 were used in calculating the diffusion coefficient D_{AB} from the Chapman-Enskog equation [25]

$$D_{AB} = \frac{1.858 \times 10^{-3} \sqrt{T^3(1/M_A + 1/M_B)}}{P\sigma_{AB}^2 \Omega_{D,AB}} \tag{15}$$

Here M_A = 40 g mol^{-1} (Ar) and M_B = 96 g mol^{-1} ($Si(OH)_4$) are the molecular weights, P = 1 atm the total pressure, the collision diameter σ_{AB} = 4.211 Å, and the collision integral $\Omega_{D,AB}$ = 0.867 was found from tabulated [27] interaction energies. The calculated value of D_{AB} is 0.64 cm^{2}s^{-1}.

The kinematic viscosity of a gas mixture is defined by

$$v_g = \frac{\eta_{mix}}{\rho} \tag{16}$$

$$\rho \approx \rho_{Ar} \tag{17}$$

where $\rho_{Ar} = 0.519 \times 10^{-3}$(g cm^{-3}) [28] is the Ar density at 650 °C and 1 atm. Since the partial pressure of $Si(OH)_4$ is very small, the Ar gas viscosity is used to calculate η_{mix}

$$\eta_{mix} = \eta_{Ar} = \frac{2.669 \times 10^{-5} \sqrt{M_{Ar} T}}{\sigma_{Ar}^2 \Omega_{Ar}} \tag{18}$$

with Ω_{Ar} = 0.826 [27]. The calculated values are $\eta_{mix} = 4.95 \times 10^{-4}$ Poise and v_g = 0.95 cm^{2}s^{-1}, yielding k_m = 0.55 cm s^{-1}.

The Schmidt number

$$Sc = \frac{v_g}{D_{AB}} \tag{19}$$

is calculated to be 1.5 which satisfies the condition

$$0.6 \le Sc \le 50 \tag{20}$$

for the applicability of Eq. (14).

The flux of $Si(OH)_4$ to the flat sample calculated from Eq. (13) is $J_{Si(OH)_4} = J_{Si} = 7.3 \times 10^{-14}$ mol cm^{-2} s^{-1} or $J_{Si} = 2 \times 10^{-12}$ g cm^{-2} s^{-1}, if $p_{Si(OH)_4}$ has the maximum (input) value of 1×10^{-8} atm. If the equilibrium state of (1) is approached and a minimum value $p_{Si(OH)_4} = 1.1 \times 10^{-9}$ atm is achieved, a lower value of the silicon flux to the sample surface, $J_{Si} = 2.2 \times 10^{-13}$ g cm^{-2} s^{-1}, results. The total Si amount deposited onto a sample surface of 1.6 cm^2 after 240 h is therefore in the range $n_{Si}^{mass\ transfer} = 1 \times 10^{-8}$ to 1×10^{-7} mol. These $n_{Si}^{mass\ transfer}$ values are sufficient to account for the amount of silicon found in the scale ($n_{Si}^{scale} = 1.3 \times 10^{-8}$ mol), but smaller than the total amount of Si transported into the reactor in the gas ($n_{Si}^{gas} = 2.1 \times 10^{-6}$ mol). It is therefore concluded that the Si impurity in the reaction gas was the main supply for the formation of silicon oxides in the Cr_2O_3 scale during oxidation in water vapour.

Silicon in the gas was deposited onto the sample surface via the chemical vapour deposition (CVD) process. Numerous parameters may affect CVD rates, such as gas

flow rate, sample direction/angle, surface roughness, nucleation sites, and so on. Surface roughness could be a significant factor. The samples had been ground to a 1200 grit finish prior to exposure. The physical shadowing of an uneven surface could cause unequal deposition on the tops and sides of grinding scratches.

Chromia scales formed in wet CO_2 gas usually have finer grains than those in dry gas, a result thought [3, 4, 29] to be due to changed diffusion properties of oxide grain boundaries. Solubility of Si in Cr_2O_3 is negligible at high temperature [30], and for this reason, SiO_2 grains have been found on Cr_2O_3 grain boundaries and triple points [3].

The discovery of chromia scale contaminations by Si during corrosion in water vapour offers a new explanation for the formation of finer Cr_2O_3 grains in wet gases. The additional, intergranular SiO_2 grains impede Cr_2O_3 grain boundary movement and hence grain growth. The growth of polycrystalline Cr_2O_3 scales is controlled by the transport of species along grain boundaries [31, 32]. The finer-grained Cr_2O_3 scales formed in wet gas have higher grain boundary densities, and these scales are on this basis expected to grow faster than those formed in dry gas. However, the intergranular SiO_2 grains formed in wet gas oxidation act as a diffusion barrier to Cr_2O_3 grain boundary species. For this reason, the Cr_2O_3 scale formed on a Si-free alloy in Ar-20CO_2-20H_2O was thinner than that in Ar-20CO_2 at 650 (Fig. 1) and 818 °C [3, 4].

Conclusions

Chromia scales containing silicon formed on a Si-free alloy exposed to Ar-H_2O gas. A diffusion calculation showed that the very low concentration of alloy silicon was insufficient to account for the level of silicon found in the scales.

Water used to generate the water vapour, either deionised or distilled, was found by chemical analysis to contain silicon. Although Si concentrations of ~ 0.16 mg/L were much lower than those of tap water, a simple mass balance calculation showed that the amount was more than enough to supply the scale Si content, if carried into the reactor tube.

The deionised and distilled water also contained low levels of dissolved F, Cl, S, and Ca. These impurities were also found in the chromia scales, indicating that water solutes were indeed carried by the gas stream into the reactor.

Water vapour was generated in a conventional laboratory bubbler. Consideration of likely water droplet sizes and also of solid residue particles resulting from their evaporation and application of Stokes' Law led to the conclusion that both droplets and particles would be carried by the flowing gas.

The partial pressure of $Si(OH)_4$ in the gas stream is low at ~ 10^{-8} atm. However, the calculation of mass transfer in the viscous flow regime showed that the rate of transfer of Si from the gas to the chromia scale surface is sufficient to account for the observed silicon uptake.

Silicon impurities in drinking water are ubiquitous. Normal quality deionised or distilled water still contains low, but significant levels. Vapour generated from these

liquids can generally be expected to convey sufficient Si to lead to significant accumulations in slow-growing oxide scales.

As SiO_2 precipitates within Cr_2O_3 scales are located at grain boundaries and triple points, they will affect the protective qualities of the scale. It seems likely that much of the published laboratory research on water vapour effects on oxidation would be affected by this phenomenon.

Acknowledgements Financial support from the Australian Research Council's Discovery Program is gratefully acknowledged.

Funding Open Access funding enabled and organized by CAUL and its Member Institutions.

Open Access This article is licensed under a Creative Commons Attribution 4.0 International License, which permits use, sharing, adaptation, distribution and reproduction in any medium or format, as long as you give appropriate credit to the original author(s) and the source, provide a link to the Creative Commons licence, and indicate if changes were made. The images or other third party material in this article are included in the article's Creative Commons licence, unless indicated otherwise in a credit line to the material. If material is not included in the article's Creative Commons licence and your intended use is not permitted by statutory regulation or exceeds the permitted use, you will need to obtain permission directly from the copyright holder. To view a copy of this licence, visit http://creativecommons.org/licenses/by/4.0/.

References

1. H. E. Evans, D. A. Hilton, R. A. Holm, and S. J. Webster, *Oxidation of Metals* **19**, 1983 (1).
2. M. J. Bennett, J. A. Desport, and P. A. Labun, *Oxidation of Metals* **22**, 1984 (291).
3. T. D. Nguyen, A. L. Fontaine, L. Yang, J. M. Cairney, J. Zhang, and D. J. Young, *Corrosion Science* **132**, 2018 (125).
4. T. D. Nguyen, J. Zhang, and D. J. Young, *Oxidation of Metals* **87**, 2017 (541).
5. T. D. Nguyen, J. Zhang, and D. J. Young, *Oxidation of Metals* **81**, 2014 (549).
6. B. A. Pint and K. A. Unocic, *JOM* **70**, 2018 (1511).
7. T. Sand, A. Edgren, C. Geers, V. Asokan, J. Eklund, T. Helander, J. E. Svensson, and L. G. Johansson, *Oxidation of Metals* **95**, 2021 (221).
8. J. F. Moulder, W. F. Stickle, P. E. Sobol, K. D. Bomben, *Handbook of X-ray Photoelectron Spectroscopy*, ed. by J. Chastain, Perkin-Elmer Corp., (Minnesota, 1992).
9. M. C. Cheng and I. B. Cutler, *Journal of the American Ceramic Society* **62**, 1979 (593).
10. E. J. Opila, D. S. Fox, and N. S. Jacobson, *Journal of the American Ceramic Society* **80**, 1997 (1009).
11. I. Barin and G. Platzki, *Thermochemical Data of Pure Substances*, (VCH, Weinheim, 1995).
12. M. D. Allendorf, C. F. Melius, P. Ho, and M. R. Zachariah, *Journal of Physical Chemistry* **99**, 1995 (15285).
13. J. Crank, *The Mathematics of Diffusion*, 2nd ed (Oxford University Press, London, 1975),.
14. R. J. Borg and D. Y. F. Lai, *Journal of Applied Physics* **41**, 1970 (5193).
15. *Quarterly drinking water quality report, Sydney Water* (2021), link: https://www.sydneywater.com.au/web/groups/publicwebcontent/documents/document/zgrf/mjm0/~edisp/dd_234949.pdf.
16. *Water fluoridation: questions and answers, NSW health* (2015), link: https://www.health.nsw.gov.au/environment/water/Documents/fluoridation-questions-and-answers-nsw.pdf
17. P. Treguer, D. M. Nelson, A. J. Van Bennekom, D. J. DeMaster, A. Leynaert, and B. Queguiner, *Science* **268**, 1995 (375).
18. R. H. Perry, D. W. Green, J. O. Maloney, *Perry's Chemical Engineers' Handbook*, 7th ed. (McGraw-Hill, 1997).
19. A. H. Woodcock, C. F. Kientzler, A. B. Arons, and D. C. Blanchard, *Nature* **172**, 1953 (1144).

20. C. F. Kientzler, A. B. Arons, D. C. Blanchard, and A. H. Woodcock, *Tellus* **6**, 1954 (1).
21. A. H. Woodcock, *Journal of Geophysical Research* **77**, 1972 (5316).
22. D. E. Spiel, *Journal of Geophysical Research* **103**, 1998 (24907).
23. https://www.engineeringtoolbox.com/gases-absolute-dynamic-viscosity-d_1888.html
24. E. T. Urbansky and M. R. Schock, *International Journal of Environmental Studies* **57**, 2000 (597).
25. D. R. Gaskell, *An Introduction to Transport Phenomena in Materials Engineering*, (Macmillan, New York, 1992).
26. R. A. Svehla, Estimated viscosities and thermal conductivities of gases at high temperatures, **NASA Technical Report R-132**, 1962 (1–120).
27. R. C. Reid and T. K. Sherwood, *The Properties of Gases and Liquids*, 2nd ed (McGrawHill Book Co., New York, 1966),.
28. https://www.engineeringtoolbox.com/argon-density-specific-weight-temperature-pressure-d_2089.html
29. J. Zurek, D. J. Young, E. Essuman, M. Hansel, H. J. Penkalla, L. Niewolak, and W. J. Quadakkers, *Materials Science and Engineering A* **477**, 2008 (259).
30. E. N. Bunting, *Journal of Research of the National Bureau of Standards* **5**, 1930 (325).
31. D. Caplan and G. I. Sproule, *Oxidation of Metals* **9**, 1975 (459).
32. R. J. Hussey, D. F. Mitchell, and M. J. Graham, *Materials and Corrosion* **38**, 1987 (575).

Publisher's Note Springer Nature remains neutral with regard to jurisdictional claims in published maps and institutional affiliations.